Journal Pre-proof

Direct extrusion 3D printing for a softer PLA-based bio-polymer composite in pellet form

Sarat Singamneni, Malaya Prasad Behera, Derryn Truong, Marie Joo Le Guen, Elspeth Macrae, Kim Pickering

PII: S2238-7854(21)00869-3

DOI: https://doi.org/10.1016/j.jmrt.2021.08.044

Reference: JMRTEC 3482

To appear in: *Journal of Materials Research and Technology*

Received Date: 2 March 2021

Revised Date: 6 August 2021

Accepted Date: 11 August 2021

Please cite this article as: Singamneni S, Behera MP, Truong D, Le Guen MJ, Macrae E, Pickering K, Direct extrusion 3D printing for a softer PLA-based bio-polymer composite in pellet form, *Journal of Materials Research and Technology*, https://doi.org/10.1016/j.jmrt.2021.08.044.

Direct extrusion 3D printing for a softer PLA-based bio-polymer composite in pellet form

Sarat Singamneni[1], Malaya Prasad Behera[1], Derryn Truong[1], Marie Joo Le Guen[2], Elspeth Macrae[2], and Kim Pickering[3]

[1]*Auckland University of Technology, Auckland, New Zealand*

[2]*Scion, Rotorua, New Zealand*

[3]University of Waikato, Hamilton, New Zealand

** Corresponding author**: Associate Professor Sarat Singamneni,** Auckland University of Technology, Auckland, New Zealand, Ph: 0064 9 921 9999 (Ext. 8002), Email: sarat.singamneni@aut.ac.nz*

Direct extrusion 3D printing for a softer PLA-based bio-polymer composite in pellet form

Abstract

Fused deposition modelling is the most popular method of 3D printing with a variety of polymers, but the raw materials are commonly in the filament form. Research has demonstrated the ability to use pellets for this process, which are easier to produce than filaments. Apart from the savings on the pre-processing, the approach also combines the good attributes of both injection moulding and 3D printing and referred to as extrusion 3D printing. Direct printing of pellets is especially suited for thermosensitive polymers, with which, repeated or excessive heating may lead to degeneration. Also, polymers that are too soft do not qualify for filament-based extrusion. PLA is a popular choice for fused deposition modelling in the filament form but is often too brittle. A softer version of PLA composite based on PBAT and cellulose fibres is proposed here for 3D printing. Considering the lack of stiffness of the filaments, direct extrusion from pellet form is evaluated. Regardless of form, the polymer material system satisfied the stringent conditions of consolidation as dictated by the dynamic combination of extrusion and rasterised material deposition. Experimental evaluation based on meso-structural and mechanical property analyses indicate the new pellet-based material system to be suitable and to perform well. The novelty of the material and process combination is that the printed samples were actually comparable mechanically to the injection moulded counterparts, which is an extraordinary achievement, considering the shortcomings typical of material consolidation in additive manufacturing.

Keywords: *polymer composite; soft PLA; pellets; extrusion; 3D printing; consolidation*

1. Introduction

Fused deposition modelling has by far been the most common additive processing approach for polymeric materials in 3D printing [1, 2, and 3]. The raw material has invariably been in the form of a filament, while ABS and PLA are the materials commonly used [4]. The filament is heated gradually, as it is fed through the print-head system and its incoming solid front acts as a piston that pushes the heated and plasticised polymer pool at the exit of the nozzle. The polymer filament must possess certain viscosity and rigidity requirements so as to achieve enough extrusion pressure and maintain the continuity of the extruded strand. The necessity to exhibit these specific attributes and the cost of converting the raw materials into the filament forms often makes it difficult to process many polymer materials by fused deposition.

Direct printing from the pellet form is a possible option, which is also amenable to including particulate and fibrous filler materials to form polymer composite material solutions. In reality, polymer material production in the pellet form is simpler and more economical [5, 6, and 7]. Extrusion printing direct using pellets then eliminates certain value-adding intermediate stages and becomes cheaper and more versatile. The main bottlenecks are the technical challenges that arise in extruding the pellets as part of the printing process, while also achieving the controlled fusion in the material substrate laid down as per the raster schemes. Consequently, extrusion 3D printing based on polymer pellets has achieved relatively less attention compared to printing using filaments.

Early efforts by Reddy et al. involved design and development of a melt deposition 3D printing system based on a screw extruder and evaluated different polymers in the pellet form based on experiments undertaken as per the Box-Behnken design [8]. Volpato et al. developed a plunger type 3D printing system for processing polymers in the pellet form and evaluated material degradation, continuity of filament fusion, product scale, and surface precision aspects with different materials [9]. Wang et al. developed a similar system and attempted high speed extrusion 3D printing of polymer pellets [10]. Liu et al. built a large-scale double-stage-screw printer for fused deposition modelling of polymers in pellet forms [11]. Experimental and analytical evaluations led to the conclusion that the system designed

and fabricated was capable of printing a variety of polymers in pellet form at much lower costs compared to the filament-based printing route.

Certain polymers are heat sensitive and lead to processing difficulties as the thermal decomposition temperatures overlap on the process windows. Zhou et al., hypothesised that the extrusion 3D printing approach direct from pellets allows to combine several process stages together, greatly reducing the risk of thermal exposure in such cases [12]. Polyvinyl alcohol, one of the heat sensitive polymers was evaluated for extrusion 3D printing in pellet forms and proved to be responding well. Elastomeric polymers also suffer from lack of rigidity during filament extrusion as in the case of traditional fused deposition modelling. Kumar et al., showed the extrusion 3D printing using raw materials in the pellet forms can overcome this difficulty and qualify elastomers such as ethylene vinyl acetate to be added to the additive processing realm [13]. Large-scale printing also becomes a case for printing direct from pellet form both economic and product lead time considerations, as was demonstrated by Moreno et al., using polymeric pellet-based additive manufacturing systems successfully to build large polymeric parts and bringing shipyard 4.0 and additive manufacturing together [14]. Additive processing by pellet extrusion was also shown to be a promising approach recycled polymer waste [15]. While these initial attempts made some progress, challenges remained; the pellet extruder is as complex as an injection moulding system and there is further complexity down-stream in terms of the kinematic relationships between the print head and the substrate table.

Wang et al. identified several shortcomings associated with extrusion 3D printing of polymer pellets [16]. One of the major challenges recognised was the need to overcome the ‘bridge’ phenomenon, where the polymer picks up air during the plasticisation process leading to instability and discontinuity in material flow. It may also cause uncontrollable flow at the nozzle tip. The end result is an uneven filament structure and consequent loss of control on the print quality. A double screw system was developed by Liu et al. to combat these problems, where the first screw mainly draws the pellets in and pushes them to the heating zone. The plasticised pool of polymer then accumulates in an intermediate chamber, from

where polymer is squeezed out of nozzle by the second metering screw. The intermediate polymer flow stages had vent holes to dissipate gases if any occurring [17].

Khondoker and Sameoto went a step further and developed, again, a two-stage extrusion system for printing polymers in the pellet form [18, and 19]. In their design, the pellet feeding, heating and plasticising process takes place in a standalone system, while the softened polymer is transferred to the print head by means of a flexible heated tubular conveyor. This separation of pellet heating and the dynamics of deposition of the polymer filament was reported to reduce the 'bridge' effects. It also clearly demonstrated that the challenges of printing polymer pellets can be overcome by simple technological innovations, thus giving further impetus to the evaluation of the potential for different polymers to be used in extrusion printing in pellet form.

Singamneni et al evaluated polybutyrate-adipate-terephthalate (PBAT) polymer composites in pellet form, for extrusion printing [20]. Varying amounts of wood flour particles were added into the polymer before pelletising. It was noted that pure PBAT offers significant resistance to printing from pellet form possibly due to its highly viscous nature in its softened form. Addition of just a small quantity of the wood flour resulted in a thixotropic behaviour, beneficial to extrusion However, excessive filler material, close to 20 % by weight, caused deterioration in extrusion quality due to coagulation at the nozzle outlet, and the build-up of back pressure within the extrusion chamber.

Based on these observations a new polymer composite material based on the combination of PLA with elastomers such and cellulosic fibres was selected for evaluation of response to extrusion printing from the pellet form. The elastomeric component PBAT softens the PLA matrix, while the presence of the cellulosic fibres in small quantities helps to develop the thixotropic nature to the extrudate. Elastomers such as PBAT present advantageous properties in some applications, however, they are more difficult to print using filament due to the conventional printer design where the solid phase of the filament pushes the molten portion through the die. In the case of an elastomeric filament, the solid portion is

often not stiff enough to push through and it can result in longer printing time and print failures. The hypothesis that the combination of PLA, PBAT, and cellulosic fibres allows to soften the PLA and also qualifies for 3D printing by the direct extrusion of the polymer composite in pellet form is tested in this study. The influence of varying process parameters was investigated experimentally and analysed by the Taguchi method. Filament consistency was established from single strand specimens. Meso-structure and mechanical behaviour were evaluated for multi-layer printed samples. Overall, the polymer composite material proved to be suitable for printing from pellets, with the coalescence and properties depending on the optimisation of the critical experimental factors.

2. Materials and Methods

PLA is produced from plant material and is considered a more environmentally friendly plastic compared to ABS. It is naturally transparent and can be coloured to various degrees of translucency and opacity. It is also stronger and more rigid than ABS but is more difficult to work with when making complicated interlocking assemblies and pin-joints. The lower melting temperature of PLA makes it unsuitable for many applications as exposure to heat might cause the component to deform but loading with suitable filler materials can resolve this to varying degrees. The polymer composite was made up of 89.8 wt.% PLA (Ingeo, Natureworks 2003D), 10 wt.% of PBAT (Ecoflex ® F Blend C1200) and 0.2 wt.% of blue-dyed cellulosic wood fibre (Tencel™Lenzing). It was produced in the pellet form, based on a 26-mm, 40 L/D ratio, scientific twin screw, co-rotating extruder LTE26-40 (Labtech Engineering Ltd, Thailand) at Scion, Rotorua, New Zealand. All materials were dried overnight at 60 °C. The extruder screw speed was 200 rpm and the feed was 15 rpm. The temperature was set to 180 °C at the first 5 zones and 185 °C at the last 5 zones. Strands were cooled in a water bath and subsequently cut into 2mm long pellets.

The basic thermal attributes of the polymer composites was established using a differential calorimetry test on a NETZSCH DSC system. The material was preheated at 60 °C for 15 minutes to remove any residual moisture that may have accumulated. An extrusion 3D printer developed at AUT was used for all the printing trials. As shown in Figure 1 (a), this system is composed of a portable polymer extrusion head mounted on a 3-axis CNC

gantry. The 3-axis CNC bed was sourced from a standard pick-and-place type mechanism used in assembly and automation tasks and rewired using open-source hardware and software systems. Stepper motors are used for driving the sliding systems along the X-, Y-, and Z-axes. The print head was designed using the injection moulding system as the basis, where a rotating screw feeds the polymer pellets along the length of the feed tube. The external ring-type resistance heater mounted at the end of the extruder tube will provide the necessary heat to soften the polymer pellets at the end of the feeder tube. Several design alternations were necessary to converge on the final dimensions of the lead screws, the length of the feeder tube, and the volume of the heating chamber in which the softened polymer collects, before being ejected through the nozzle, in the form of a filament.

Based on the screw-type extrusion head design, two critical process parameters arise. First, the speed of rotation of the stepper motor that drives the lead screw, which in turn feeds the fresh polymer pellets towards the heating chamber controls the speed of extrusion of the polymer filament. The maximum temperature setting on the resistance ring heater used around the heating chamber will allow to control the temperature of the extruded filament. This is a critical parameter as this temperature of the extruded filament has to be set to achieve the thixotropic nature for the polymer filaments deposited on the substrate. The extrusion speed has to be synchronised with the speed of movement of the print head along the X- and Y- directions, in order to maintain the same speed of printing of the softened polymer filament on the substrate. The three critical parameters thus arising, extrusion speed, the nozzle temperature and the speed of printing (speed of movement along the X- and Y-directions) need to be synchronised closely in order to achieve a polymer filament in the exact thixotropic state as necessary to achieve sufficient inter-strand and inter-layer coalescence and the formation of the 3D printed shape with sufficient dimensional and mesostructural controls.

Sufficient mechanical forces must be applied through the material transferring mechanism, in order to allow for the spindle to continually extrude the softened polymer material. If there is any excessive plasticisation of the material all along the nozzle, it will get highly viscous and will begin sticking to the spindle, resulting in a lack of flow. To avoid this, the material should only be melted at the bottom part of the nozzle, where it is extruded onto the print bed, allowing the material in the upper sections of the nozzle to remain in the solid-state. The solid materials provide adequate mechanical forces to push out the viscous material as it will not adhere to the spindle. At the same time, this mechanical movement pushes the solid-state material towards the heating element, turning it into a viscous material before it gets printed onto the bed.

An Arduino mega 2560 motherboard was installed to control motions along X-Y-Z axes, spindle rotation, and the heating element of the extruder barrel. The open source Repetier-Host Windows 2.1.6 version software was used to integrate the communication between the motherboard and the driving elements. An aluminium base plate with a JCS heating element of a temperature range up to 250 °C mounted at the bottom was used on top of the print bed to provide the necessary control over the envelope temperatures. Initially, the printing speed and spindle rotation were automatically set to some default values by the slicer module of the software. After a few trial and error runs, the printing and spindle rotational speeds were optimised at 40 mm/sec for the best quality deposition of the filament and was maintained at these levels subsequently.

The distance between the nozzle tip and the print bed (air gap) is also predetermined by the software during slicing, assuming the raw material to be in the filament form. A properly optimised air gap is needed, however, to accommodate the greater size variations in the filament emanating from pelleted raw materials. The air gap must be slightly more than normal, to accommodate for the greater variations in the printed strand sizes. Over-sizing the air gap would result in the filament becoming wavy or being stretched, while under sizing would cause the filament to be flattened by the nozzle and/or scraping of the material. After a few trials, the optimum air gap was identified to be 1.2 mm which was then maintained for this research.

Extrusion trials were conducted depositing single strand filaments, to identify the best extrusion chamber temperature. Based on the observations of continuity and consistency of the filament extruded and printed, the best extrusion head temperature for the experimental material was identified to be 200 °C. A single layer specimen of dimensions 50 x 20 mm was then printed to further substantiate the extruder head temperature, while also optimising the base plate temperature. Based on these observations, the optimum nozzle temperature was confirmed as 200 °C. Also, observing the inter-strand coalescence within the single layer specimens, the optimal base plate temperature was 110 °C. Multi-layer samples of dimensions as shown in Figure 1(b) were then printed to evaluate the interactions, if any, between process parameters. From these initial printing trials, the best extrusion head and baseplate temperatures were confirmed to be 200 °C and 110 °C. These temperatures allowed both sufficient consistency of the filament and quality of inter-strand and inter-layer coalescence.

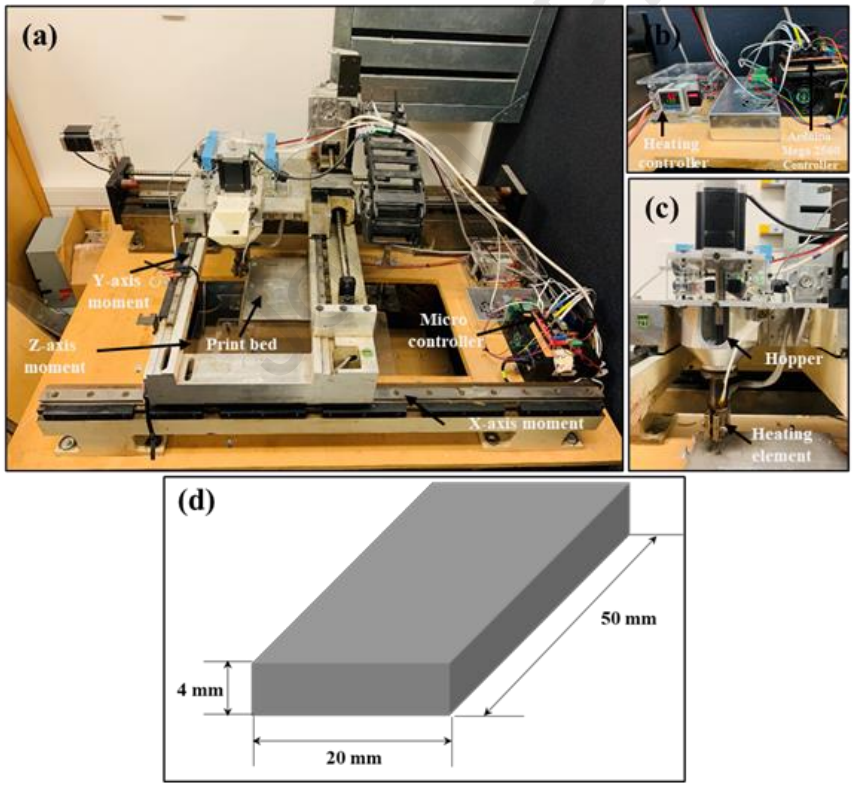

Figure 1. (a) Extrusion 3D printing set-up developed at AUT; New Zealand (b) the hardware and control system, (c) close=up view of the extrusion head and (d) CAD model of the samples produced

With the best possible options for the critical parameters identified, the next step was to evaluate the influence of these parameters on the critical responses of the printed samples. Three specific parameters, print speed, extrusion and envelope (bed) temperatures were identified to be critical. This was based on a number of trial and error attempts printing samples with varying conditions, followed by naked-eye inspection of the consolidation mechanics. An experimental design based on the Taguchi method was developed for evaluating the material and process interactions [21]. With the three experimental parameters: nozzle temperature, print-bed temperature, and print velocity set at three different levels each, the Taguchi L9 experimental design was progressed, in order to reduce the total number of experiments to a minimum. The experimental design together with the values of the process parameters at the three levels selected are presented in Table 1.

The meso structures resulting from fused deposition modelling often lead to inferior material consolidation and anisotropic property responses and the printed parts are generally inferior to the injection moulded counterparts [22]. A set of injection moulded samples were also produced to benchmark results and to compare the properties of the 3D printed test pieces. In order to maintain comparable thermal conditions, the injection moulded samples were also produced with the same nozzle temperature settings at 190, 200, and 210 °C. A bench-top manual injection moulding equipment Mini Molder available at AUT was used for this purpose. CNC milled aluminium dies producing three-point bending samples of the same dimensions as the printed samples stated above were used to produce the comparative test coupons.

Table 1. Taguchi L9 experimental design

No.	Nozzle Temp. (°C)	Bed Temp. (°C)	Print Velocity (mm/s)
D1	210	180	30
D2	210	160	40
D3	210	140	50
D4	200	180	40
D5	200	160	50
D6	200	140	30
D7	190	180	50
D8	190	160	30
D9	190	140	40

Three-point bend testing was used as a representative means of establishing the mechanical properties of printed samples. The specimen used in the current experimental investigations was designed based on the ASTMD790 standard for flexural modulus test based on 3-point bending. The recommended dimensions as specified in the standard are 100mmX25mmX3mm. However, some flexibility is allowed in these dimensions and based on the printing constraints and other limitations as imposed by the compression testing equipment available the authors have used the 50mmX20mmX4mm dimensions. The results are comparable to any other similar such experiment done on the same materials processed using the same printing methods. Prior to testing, the length, width, and thickness dimensions of the samples were recorded. During the test, the rectangular samples were placed horizontally on two custom-designed fixed supports and loaded centrally. A support span of 25 mm was used. To avoid the non-homogeneous meso-structural regions, the 50 mm sample had each end removed. The loading rate used was 2 mm/s and was applied until the deflecting sample was in contact with the support structure. Based on the results of the tests,

the maximum stress and strain and the flexural modulus values were calculated using the equations from the theory of bending. The ratio of deflection for a given force was obtained by measuring the gradient of the force/deflection curve in the elastic region.

3. Results and Discussion

3.1. Thermal analysis

The DSC curve resulting from the thermal analysis of the current polymer pellets is shown in Figure 2. The first smaller transition attained is indicative of the glass transition temperature of PLA at around 60 to 70 °C, while the large exotherm peak is indicative of a melting transition around 158 °C as indicated in Figure 2. This was used as the basis to identify the nozzle temperature settings for the experimental trials, as discussed in the methodology section. Considering the wide gap between these two peaks, this polymer composite offers a wide window of opportunity for the dynamic consolidation mechanics typical of the additive manufacturing methods. It should be relatively easy to maintain the thixotropic constraints during the course of coalescence, with varying process conditions.

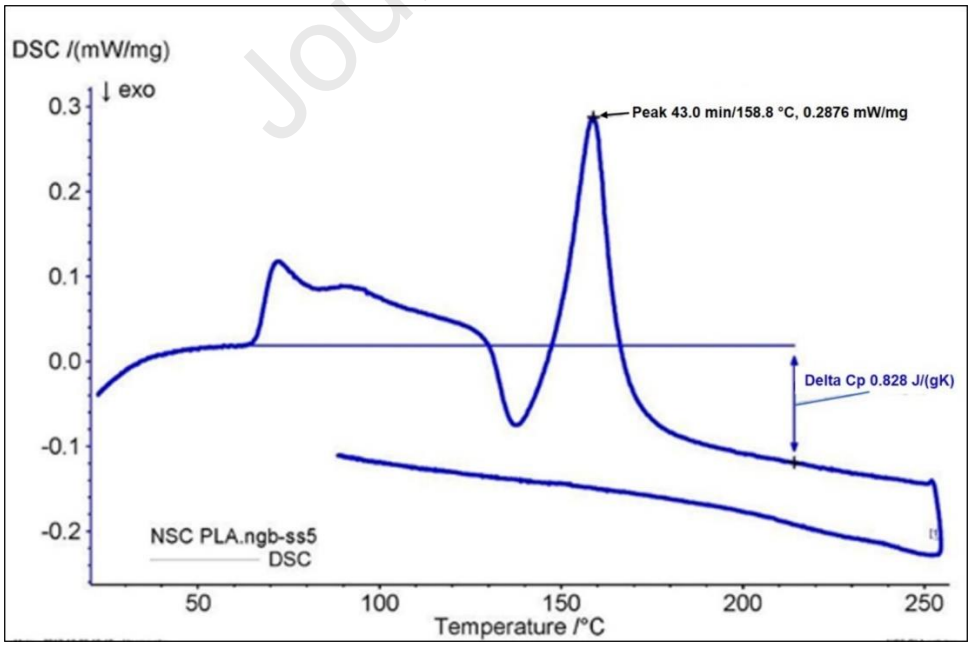

Figure 2. Differential scanning calorimetry (DSC) results

3.2. Filament continuity, single and multi-layer printing

To remove moisture that may have been absorbed from the environment, the material was preheated in an oven at 60 °C for 15 minutes prior to printing. This was to avoid problems relating to possible dimensional changes of the polymer filaments [23] as well as voids that may have resulted in the printed material. Several initial trial runs were undertaken involving printing single strands in continuous raster paths as displayed by the image in Figure 3 to ascertain the extrusion and print speed conditions for achieving the best quality strands. Insufficient thermal energy in the filament can cause premature solidification and lack of inter-strand coalescence. Excessive heating, on the other hand may lead to a reduction in the viscosity of the polymer strand, causing loss of the desired cylindrical form in the thixotropic state. Both the extrusion head temperature and the print-bed temperature settings as discussed in the previous section were ascertained based on consideration of the filament quality. The strand quality also depends on the extrusion and printing velocities and how the two are synchronised to maintain a constant cross-sectional dimension for the filament. A faster extrusion rate with a slower printing speed results in material accumulation and bulging, while a faster printing rate compared to the rate of extrusion could lead to excessive stretching and loss of the cross-sectional dimension of the printed filaments. The optimised extrusion speed and the print velocity combination as stated in the previous section are finally applied by adjusting the parameters in the software interface.

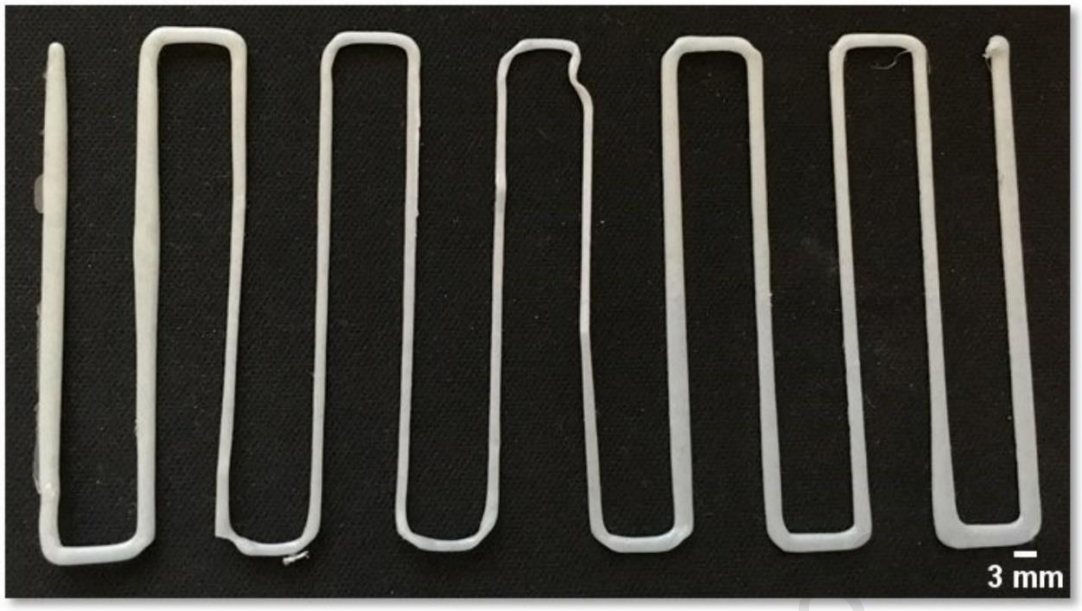

Figure 3. Single printed strands and continuity

Single layer samples were printed to observe the sintering characteristics and ascertain how the process parameters affect the overall quality. A simple parallel strand structure with zig-zag raster path format was initially chosen for the printing of layers, as this would help to reduce non-homogeneous meso-structural patterns. However, the open software platform used only allowed a few pre-set in-fill patterns to be used. After a few trial and error attempts, the continuous, radially inward raster path style as depicted in the image of the final printed sample in Figure 4 was employed. This pattern did not eliminate the meso-structural in-homogeneities altogether. In the central portion indicated as region B in Figure 4, there were parallel strands, giving rise to the uniform rectilinear meso-structures, very close to the desired patterns. However, the two end regions marked as A and C have mesostructures oriented in both x- and y- directions. To eliminate this problem, the regions marked as A and C were sliced off of the printed samples, and the remaining rectangular portions identified as B were used for the three-point bending tests.

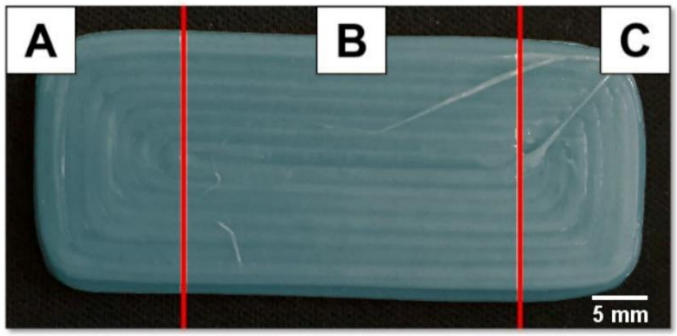

Figure 4. Raster path patterns and a single layer printed sample

With multi-layer printing, the print bed needs to be heated, as the sample may cool down prematurely, leading to shrinkage and lifting from the bed. This issue is particularly problematic during the printing of multilayer samples, as the heat from the platform is not sufficiently transferred through to the upper layers due to insufficient thermal conductivity of the polymer substrate. This caused the sample to rise off the bed during the printing of subsequent layers, which brings the sample to come into contact with the nozzle, resulting in damage. Increasing the base temperature beyond a certain limit will cause the polymer to be too soft and loose dimensional stability. Ideally, the envelope temperature should be just below the glass transition temperature to keep the filament in a semi-solid state. It was difficult for the base temperature to be controlled for multilayer samples, as there was no enclosure for the print chamber and the printed substrate was exposed to ambient environmental conditions. Due to the open-bed configuration and the consequent continuous loss of heat, it was noticed that a bed temperature at around 150 °C allowed coalescence of a few printed layers, keeping the polymer layers in the thixotropic state for the necessary time frames.

An infrared camera was used to confirm if the temperature readings of both the nozzle and the baseplate were actually matching the selected levels. Figure 6 displays the temperature differences between the pre-set values and the actual infrared measurements. The base temperature and nozzle temperatures were set to 140°C and 210°C respectively, where Figure 5(a) and 5(b) indicate a variation by around 5^{o}C in each case. A piece of masking tape was placed on top of the objects before measuring the temperate, as the metal had a reflective

nature with a high emissivity, which may lower the accuracy of the device. The masking tape provided a matte finish, with a similar emissivity to the infrared camera setting. The extrusion temperature displayed by the software was measured by placing a thermocouple between the heating element and the nozzle. However, the heating element was located near the bottom of the extrusion nozzle. This meant that only a small portion of the nozzle was actually heated to the specified temperature, while the infrared camera reading looked at the average temperature rise of the whole surface of the nozzle.

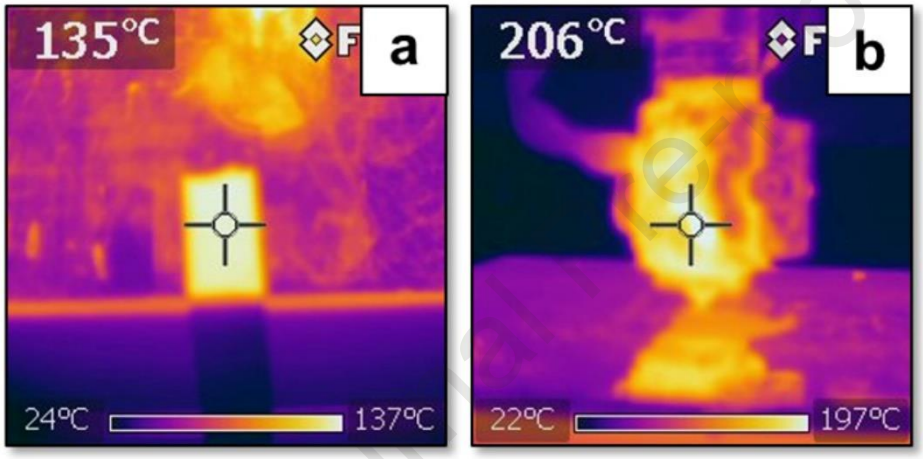

Figure 5. Infrared images(a) base plate, and (b) nozzle head.

With the critical process conditions fixed as discussed, the test coupons were printed as per the dimensions stated in the previous section with three layers each, following the experimental plans presented in Table 1 (images of the printed samples presented in Figure 6). The inter-strand coalescence and the general consolidation of the layers varied significantly as the critical process parameters were varied. It is clearly evident that the samples D1, D2, and D3 resulted in the best intra-layer consolidation. Apparently, the nozzle temperature at the highest limit, 210 °C, worked best in terms of filament consistency and the quality of printed layers, with the other parameters set at any level. In particular, the sample corresponding to the D2 trial, printed with the highest nozzle temperature, with the medium bed temperature and print speed settings resulted in the best inter-strand coalescence.

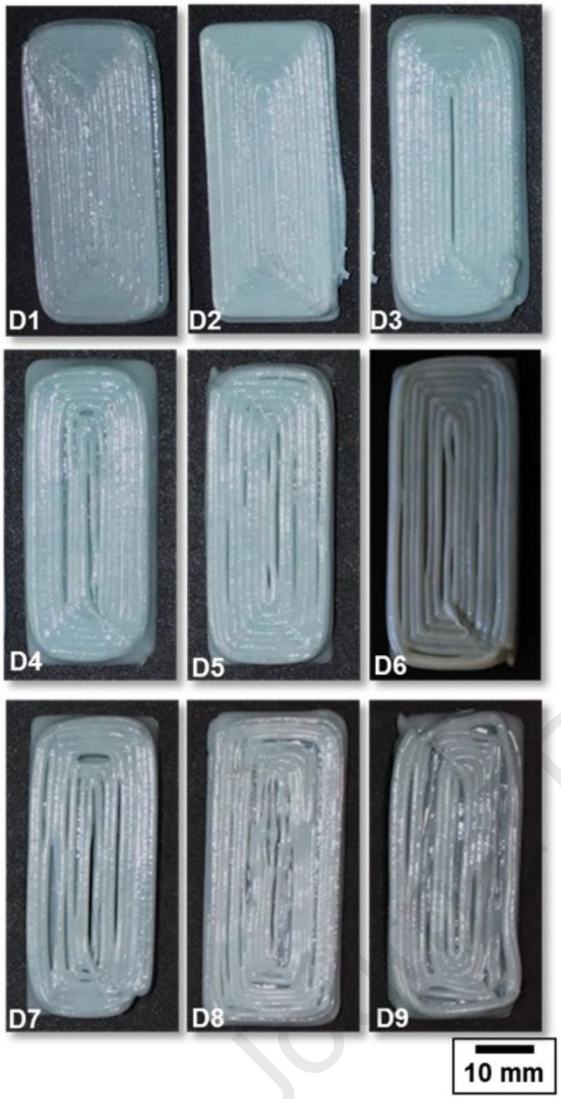

Figure 6. Multi-layer samples printed as per the design table.

3.3. Dimensional quality

Digital calliper measurements were used to establish the average values the three critical dimensions, length, width, and thickness of the samples printed. The deviations of these average values from the CAD model settings were used to establish the percent deviations between the actual and theoretical dimensions as listed in Table 2. The negative values indicate the percent reduction in size while the positive values represent the percent expansion. Overall, the width and the thickness are the worst affected dimensions. Reduction

of a dimension during printing is associated with the shrinkage of the polymer during solidification, which is a common phenomenon causing deviations in the dimensions of printed samples. The main causes for the expansion are the deposition of excessive material during extrusion and lateral flow. Excessive material deposition occurs at the end points of raster paths, where the print head either stops or reverses or changes the direction of printing. The dwell period, without any compensation in the polymer extrusion settings leads to the deposition of excess material and consequent enlargement of the layers. The lateral flow is a result of the temperature and viscosity relationships.

The shorter raster paths that occur along the relatively smaller width direction are likely to be the worst affected due to this, leading to an enlargement of the printed sample in the lateral direction showing positive values for the variation in the widths of all printed samples (Table 2). Along the length, the overall variation is dictated by the balance between the level of shrinkage and the excessive material deposition during the dwell periods at the end points. As evident from the last column of Table 2, these variations are smaller and also range from positive to negative values, depending on the differences in the strand structures due to process conditions. The variation in the thickness occurs due to either the void formation from the moisture and enlargement of the size of the filament or the weight of the layers compressing the specimen to varying degrees, (Table 2).

Table 2. Dimensional variations of samples printed as per the experimental design

No.	Thickness (%)	Width (%)	Length (%)	Coalescence (%)
D1	9.91	17.93	2.89	100
D2	9.71	11.23	4.80	88.71
D3	11.89	12.43	1.85	95.32
D4	13.79	13.76	0.10	86.72
D5	-10.80	8.21	-0.36	80.54
D6	-4.44	8.80	-1.46	98.43
D7	-13.64	10.91	-3.05	71.67
D8	-14.94	5.26	-1.69	79.23
D9	-0.25	5.26	-1.69	59.60

3.4. Inter-strand sintering, micrography, and coalescence factor

The viscosity levels and the variations in the same with temperature and other conditions have a direct bearing on the printability of a polymer. Along with the fluid flow behaviour, viscosity also dictates success in inter-strand sintering. It is ideal to have lower viscosity during extrusion, promoting continuous flow and relatively higher viscosity after printing. During consolidation, the viscosity gradually increases as the temperature of decreases, and solid-state sintering potentially takes over, to consolidate the substrate into the final form, without drastic losses in dimensions. The ability of the polymer to maintain an appropriate viscosity level through the different stages of printing controls the quality of sintering, which will eventually impact the mechanical properties of the printed components. The tack characteristics are inversely proportional to the elastic modulus of the material and should be high enough that the adhesive surfaces bond together from mere contact and slight pressures emanating from strands laid on the substrate and against one another [24]. The molecular weight and the density of the polymer will influence the inter-layer pressures and consequent coalescence. Thixotropic materials have an increased viscosity in a state of rest and a

decrease in viscosity when submitted to a constant shearing stress [25]. The constant stress applied during the extrusion process should provide enough impetus for the polymer to reduce the viscosity sufficiently so that it can overcome the frictional resistance and flow. Once settled on the substrate, the viscosity should be lowered sufficiently to promote solid state sintering.

Coalescence is a measure of the bond quality between the printed polymer strands. Frenkel's model of sintering provides a means to evaluate the quality of formation of bonds in fused deposition by extrapolating the theory from consolidation of particles to continuous strands. Molecules migrate between strands, moving between vacancies in the crystal structure and leading to coalescence between strands [26]. Tack is instantaneous adhesion, but coalescence is a time-dependent process of forming bonds between adjacent strands [27, 28]. Frenkel's model suggests sintering to progress in stages, such as wetting, molecules moving towards an adsorptive equilibrium, and diffusion across the interface and then randomisation. Equating the energy of dissipation by the viscous flow to the rate of energy released by surface reduction, Frenkel's model can be used to predict the neck growth between strands. It shows that the neck growth is proportional to the time in contact and the surface tension of the polymer, while it is inversely proportional to the viscosity of the polymer. However, assuming a spherical or cylindrical form for the strands is oversimplification, as different polymers respond to the printing process in different ways. Less viscous polymers may rapidly lose their cylindrical shape and flatten upon deposition compared to polymers that are more viscous. The meso-structure left behind is representative of the partial sintering and the loss of cylindrical form of the strands due to the self-weight and can be used to apply Frenkel's model to predict the coalescence factors in extrusion printed substrates as was implemented by Alaimo et al. [29].

The SEM image of the sectioned surface of one of the printed samples is presented in Figure 7 (a). It may be observed that the polymer strands resisted slicing by a sharp knife. The serrated and stretchy bits of impressions and material remains indicate that strong intra-strand polymerisation and inter-strand sintering. The EDS results conducted on a representative

printed specimen are presented in Figure 7 (b). The element compositions are in accordance with the locations on the sectioned specimens

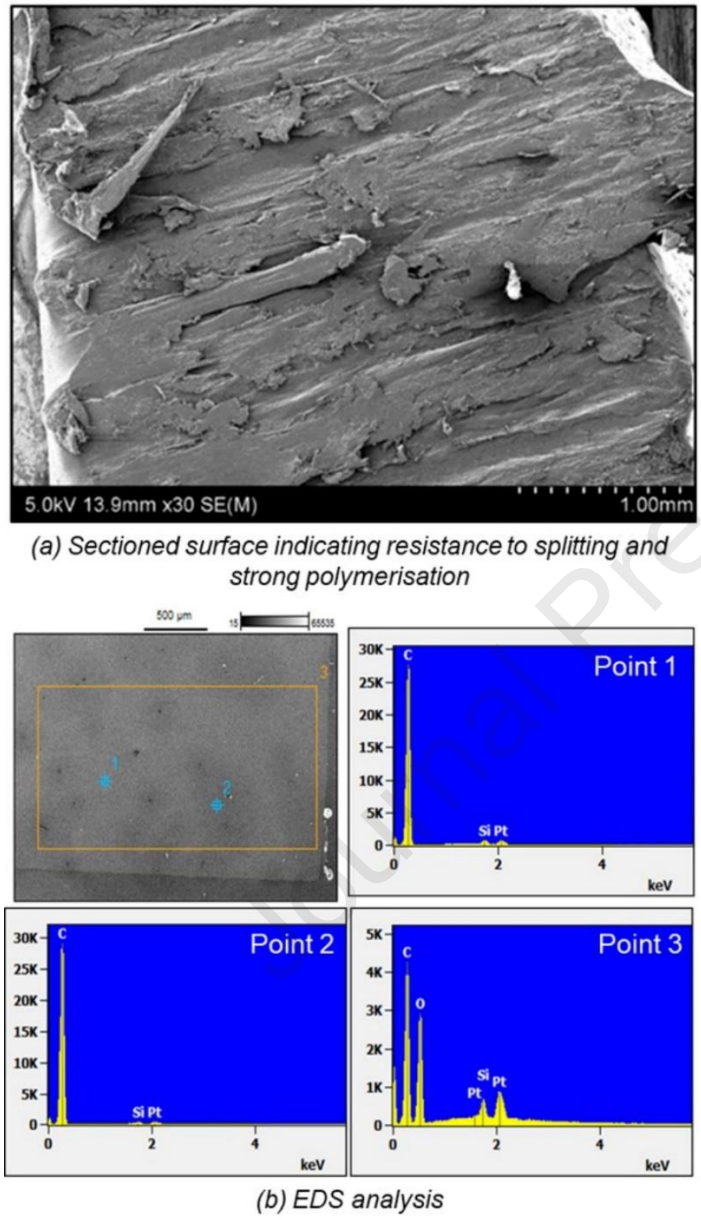

Figure 7. SEM analysis of the cross section of a representative printed specimen

Optical photomicrographs of the cross-sections of the printed samples shown in greyscale in Figure 8 are used for evaluating the mesostructures and understanding the relative coalescence levels. To establish the sintering (bond) quality of the sample, a

coalescence factor (γ) is used as a measure of the wetting (contact) region between two individual strands relative to the diameter of the strands. The two end-portions of the printed specimens indicated as Regions A and C in Figure 4 were sliced out and their cross sections were used for the meso-structural evaluations. Magnified images of the cross-sections of printed samples were used to identify the shadowy boundaries of the sectioned strands as elongated circular forms. Though hazy in places, representative lengths of the neck dimension a and the height D of the strands were measured at different locations. The coalescence factor (γ) was calculated as the ration a/D at different locations along each layer and the average and the least values based on three repeated measurements are listed in Table 2.

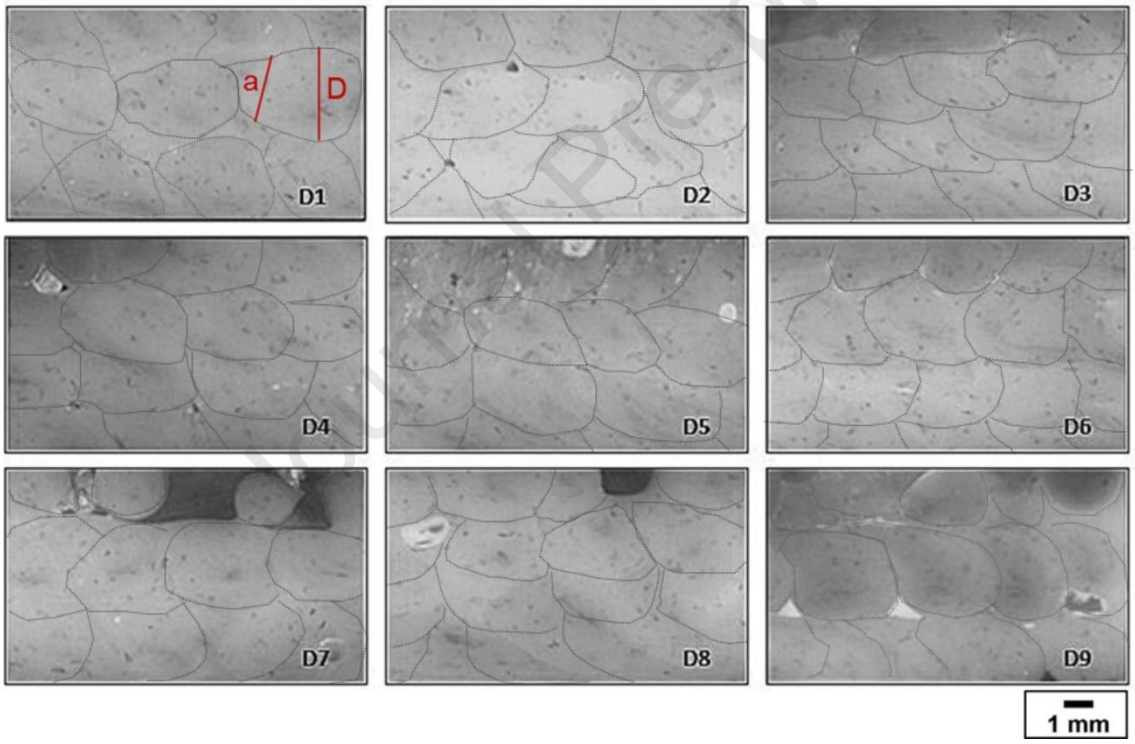

Figure 8. Meso structures of the cross sections of samples printed as per the experimental design

The coalescence factors, representative of the percentage of consolidation across different strands and layers (Table 2) indicate that the best formation of the layers occurred in the first experimental case D1. This corresponds to the maximum nozzle temperature of 210

°C, maximum bed temperature 160 °C and the lowest print speed, 30 mm/s. D2, where the bed temperature and print speed are at medium levels, while the nozzle temperature is still at the maximum level was next best. The physical forms of the printed samples (Figure 6) also confirm these two cases as the best specimens.

3.5. Three Point Bend Testing

Images of the samples subjected to three-point bending tests as described in Section 2 are presented in Figure 9. The maximum deflection, stress, strain, and flexural modulus values are listed in Table 3. The compressive force variation is influenced by the effective thickness of the sample after printing, apart from the inherent quality of the material consolidation in a given sample. The maximum deflection is also likely to vary with the thickness, which may change during printing. The samples corresponding to the experimental cases D1 to D3 had the highest maximum compressive loads (ranging 831-851 N). The maximum deflection values were also in the higher levels for these samples, varying from 1.8 to 2.0. Samples D5 and D6 exhibited the maximum bending stress (89 and 96 MPa), followed by sample D8 (80 MPa). The same trends were reflected in the flexural modulus values at around 1900-2000 MPa for D5 and D6 and around 1200 MPa with D8, almost at double the values obtained with the other samples. Both samples D5 and D6 were printed using a nozzle temperature of 200 °C with high and low print speeds respectively. Sample D4, which was printed using the same nozzle temperature and with an intermediate print speed, had a significant reduction (roughly 50 % less) in its flexural modulus.

The bed temperature also appears to have a significant role in controlling the consolidation mechanics. Samples from tests D4 and D9, had a significantly lower flexural modulus than their counterparts produced using almost the same extrusion (nozzle) temperature, which was also reflected in their maximum stress responses. It may also be noted that both these samples were printed with a print (travel) speed of 40 mm/s. The lower bed temperature appears to be the critical factor here, as it may have adversely affected the coalescence between strands and layers. The depleted strand structure from sample D9 in Figure 6 clearly reflects this, while sample D4 looks similar outwardly, could have had the internal layers demonstrating a lack of consolidation and cross linking. Overall, the

mechanical properties appear to be at the maximum possible levels with the mid- levels of printing speed, 40 mm/s in the last two sets of samples, with nozzle temperatures 200 °C and 190 °C.

Figure 9. Samples after the three-point-bend test

Table 3. Flexural test results and mechanical properties

No.	Force (N)	Maximum Deflection (mm)	Maximum Stress (MPa)	Maximum Strain	Flexural Modulus (MPa)
D1	848	1.8	66	0.0767	1,182
D2	831	2.0	71	0.0829	1,113
D3	851	1.9	68	0.0828	1,040
D4	579	1.5	43	0.0668	843
D5	677	1.7	89	0.0589	2,096
D6	820	1.7	96	0.0625	1,902
D7	432	2.1	58	0.0710	1,114
D8	545	1.7	80	0.0568	1,836
D9	434	2.0	48	0.0766	850

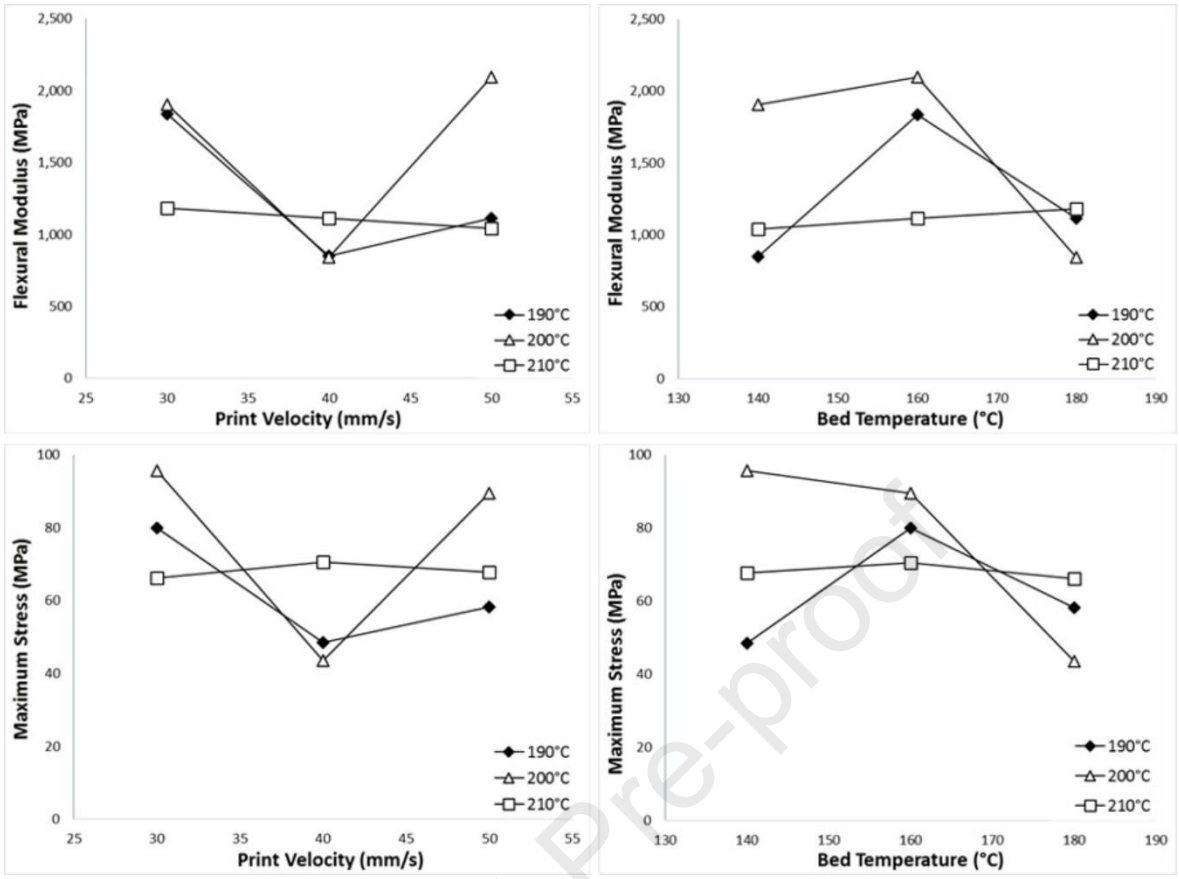

Figure 10. Flexural modulus and maximum stress responses against print velocity and bed temperature

The flexural modulus and maximum bending stress values are plotted against critical process parameters in Figure 10. The graphical visualisation of these results can now be used to converge on the best working conditions based on the results of the experiments conducted according to the Taguchi L9 experimental design. As evident in Figure 10 (a), the flexural modulus value either slightly reduces or drastically reduces, attains a minimum and then raises with increasing print velocity from 30 to 50 mm/s, at different nozzle temperatures. Figure 10 (b) is a reversal of this trend, as the flexural modulus either gradually stays almost constant or raises initially and then decreases as the bed temperature is increased. Very similar trends are reflected in the maximum bending stress with varying print velocity and bed temperature conditions, as evident in Figure 10 (c) and (d). Evidently, the print velocity and the two critical temperature factors are interacting quite intricately, and the optimum conditions can only be approximated within the limits of this fractional experimental plan based on the Taguchi L9 design. The main effects plots shown in Figure 11 can be used for

this purpose. It is clear that both maximum bending stress and the flexural modulus values are at the highest with the medium nozzle and bed temperatures. However, the print velocity at the lowest level 30 mm/s is giving the best values for both responses. Based on the signal to noise ratios, it was found that both print velocity and nozzle temperature play the most significant roles, and hence the optimum process parameters based on the Taguchi L9 experimental design are nozzle temperature 200 °C, bed temperature 160 °C, and print velocity 30 mm/s. The signal-to-noise ratio plots based on the 'nominal is the best' criterion as presented Figure 11 (c), also confirmed this choice as the best combination of process parameters.

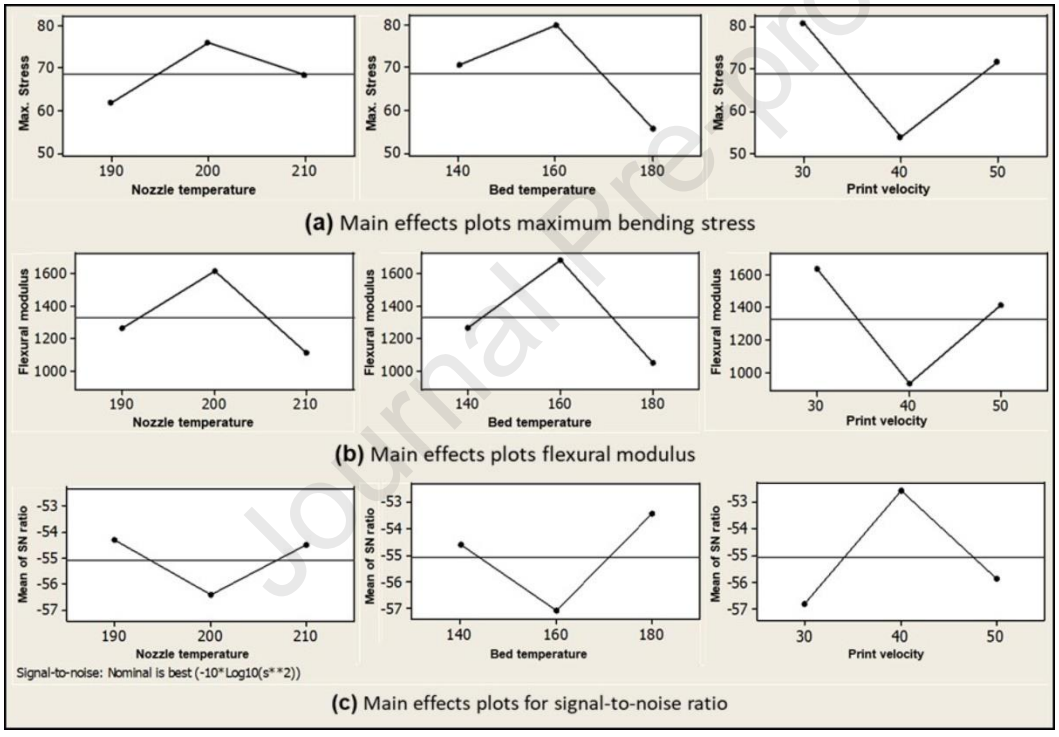

Figure 11. Main effects plots for mean (a) maximum bending stress and (b) flexural modulus (c) signal-to-noise ratio

3.6. Extrusion printing vs injection moulding

Four identical samples were printed through polymer extrusion using the optimised process conditions as stated in the previous section and their images are presented in Figure 12 (a), marked T1 to T4. To compare the relative performance of extrusion printing, three samples

were produced using a bench-top injection moulding system using the same nozzle temperature settings 190, 200 and 210 °C and included as images J1 to J3, in Figure 12 (b). The percent error in thickness, maximum compressive force, maximum deflection, bending and flexural stress, and maximum deflection values obtained from the three-point bending tests are listed in Table 4. It may be noted that the dimensions of printed samples were adversely affected due to higher bed temperature, in particular, the width of samples (Table 4). In fact, controlling the substrate temperature through a heating platform is only a temporary solution and when fully proved, commercial implementation if any, would be through a controlled envelope temperature achieved through controlling the temperature in the whole build chamber. The uniform heating thus achieved through the chamber atmosphere will eliminate the overheating of the lower layers and subsequent collapsing under the weight of the upper layers, leading to the loss in dimensional stability.

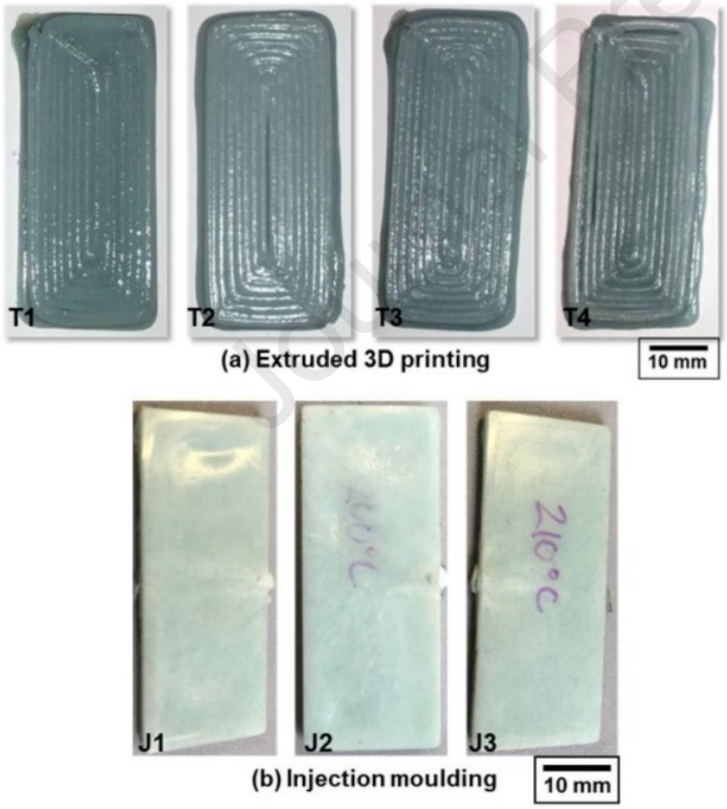

Figure 12. Three-point bending specimens produced by (a) extrusion 3D printing with nozzle temperature 200 °C, bed temperature 160 °C and print speed 30 mm/s (b) injection moulding with Nozzle temperatures 190 °C, 200 °C, and 210 °C.

Table 4. Comparative responses of extrusion 3D printed and injection moulded samples

	Extrusion 3D printed					***Injection moulded***			
Sample no.	T1	T2	T3	T4	Avg.	J1	J2	J3	Avg.
Percent error in thickness	2.75	-3.50	1.75	-1.50	-0.125	0	0	0	0
Force (N)	577	822	680	598	669	581	621	451	551
Max. Deflection (mm)	1.5	1.8	1.3	1.4	1.5	1.6	1.55	1.25	1.47
Max. Stress (MPa)	63	69	67	65	66	68	73	53	65
Max. Strain	0.0215	0.0327	0.0245	0.0219	0.0251	0.0614	0.0595	0.0480	0.056
Flexural Modulus (MPa)	1,516	1,447	1495	1410	1467	1,373	1,628	1,322	1441

The lack of control on the thermal conditions as explained above has resulted in the variations in the thicknesses of the samples as evident in the percent error in thickness values listed in the first row of Table 4 for the repeated extrusion printed samples T1 to T4. These deviations have resulted in the variations in the maximum force values as listed in the second row of Table 4 for the samples T1 to T4. However, the maximum stress and the flexural modulus values are calculated giving due consideration to the variations in the thicknesses of the repeated samples and so, the maximum deviation from the central value is very small and within the normal statistically acceptable limits. Similar observations can also be made comparing the variations in the maximum deflection and strain values listed in Table 4 for the repeated T1 to T4 extrusion printed samples.

The average compressive load withstood by the printed samples is actually higher than that with the injection moulded samples. The longitudinal strand structure and also the variations in the thickness could have caused this. Further, the extrusion 3D printed samples scored slightly higher than the injection moulded samples in terms of all other responses. This is quite an unexpected result as 3D printed samples normally exhibit inferior properties compared to injection moulding caused by meso-structural issues and the presence of inter-

strand cavities. However, in the case of the PLA-based polymer composite investigated here, the meso-structural analysis based on the optical micrographs of Figure 8 clearly indicated complete coalescence using one combination of different parameters (D6). The polymer composite performed well for extrusion 3D printing from pellet form, and also showed potential to perform better than injection moulded composites.

4. Conclusion

A polymer composite based on PLA, elastomers, and cellulosic fibres was evaluated for 3D printing by direct extrusion of raw materials in the pellet form. Experimental evaluation of meso- and microstructures and the dimensional variations identified the best range of the critical process parameters, print speed, and nozzle and bed temperatures to achieve sufficient coalescence between adjacent strands and layers. Mechanical property evaluation based on experiments conducted as per the Taguchi L9 design indicated the best combination of the critical process parameters. Evaluation of the mechanical properties of specimens printed using the best process parameter combinations compared with the injection moulded counterparts clearly demonstrated similarities between the two. Overall, the PLA, elastomer, and cellulosic fibre polymer composite proved to be a potential candidate for pellet-based extrusion 3D printing. The following are specific conclusions:

- Within the limits of the ranges of experimental factors considered in the current evaluation, the best process conditions for extrusion 3D printing of the PLA-based polymer composite are print speed 30 mm/s, nozzle temperature 200 °C, and bed temperature 160 °C.
- The average values of maximum bending and flexural stresses of specimens printed with the optimum process parameter combination are 66 MPa and 1467 MPa respectively.

- The average values of the same maximum bending and the flexural stress values of specimens produced by injection moulding are 65 MPa and 1441 MPa respectively.
- The extrusion 3D printed samples exhibited 1.6 % and 1.8 % higher maximum bending and flexure stresses compared to the injection moulded counterparts.

Acknowledgement

This research is supported by the National Science Challenge Science for Technological Innovation (SfTI) grant by the Ministry of Business, Innovation and Employment (MBIE) of the New Zealand government Grant No: CINNO1901.

References

[1] Daminabo, S. C., Goel, S., Grammatikos, S. A., Nezhad, H. Y., & Thakur, V. K. (2020). Fused deposition modeling-based additive manufacturing (3D printing): techniques for polymer material systems. *Materials Today Chemistry*, *16*, 100248.

[2] Turner, B. N., Strong, R., & Gold, S. A. (2014). A review of melt extrusion additive manufacturing processes: I. Process design and modeling. *Rapid Prototyping Journal*.

[3] Vyavahare, S., Teraiya, S., Panghal, D., & Kumar, S. (2020). Fused deposition modelling: A review. *Rapid Prototyping Journal*.

[4] Hafsa, M. N., Ibrahim, M., Wahab, M., & Zahid, M. S. (2014). Evaluation of FDM pattern with ABS and PLA material. In *Applied Mechanics and Materials* (Vol. 465, pp. 55-59). Trans Tech Publications Ltd.

[5] Parandoush, P., & Lin, D. (2017). A review on additive manufacturing of polymer-fiber composites. *Composite Structures*, *182*, 36-53.

[6] Popescu, D., Zapciu, A., Amza, C., Baciu, F., & Marinescu, R. (2018). FDM process parameters influence over the mechanical properties of polymer specimens: A review. *Polymer Testing*, *69*, 157-166.

[7] Boparai, K. S., Singh, R., & Singh, H. (2016). Development of rapid tooling using fused deposition modeling: a review. *Rapid Prototyping Journal*.

[8] Reddy, B. V., Reddy, N. V., & Ghosh, A. (2007). Fused deposition modelling using direct extrusion. *Virtual and Physical Prototyping*, *2*(1), 51-60.

[9] Volpato, N., Kretschek, D., Foggiatto, J. A., & da Silva Cruz, C. G. (2015). Experimental analysis of an extrusion system for additive manufacturing based on

polymer pellets. *The International Journal of Advanced Manufacturing Technology*, *81*(9-12), 1519-1531.

[10] Weng, Z., Wang, J., Senthil, T., & Wu, L. (2016). Mechanical and thermal properties of ABS/montmorillonite nanocomposites for fused deposition modeling 3D printing. *Materials & Design*, *102*, 276-283.

[11] Liu, X., Chi, B., Jiao, Z., Tan, J., Liu, F., & Yang, W. (2017). A large- scale double-stage- screw 3 D printer for fused deposition of plastic pellets. *Journal of Applied Polymer Science*, *134*(31), 45147.

[12] Alaimo, G., Marconi, S., Costato, L., & Auricchio, F. (2017). Influence of meso-structure and chemical composition on FDM 3D-printed parts. *Composites Part B: Engineering*, *113*, 371-380.

[13] Zhou, Z., Salaoru, I., Morris, P., & Gibbons, G. J. (2018). Additive manufacturing of heat-sensitive polymer melt using a pellet-fed material extrusion. *Additive Manufacturing*, *24*, 552-559.

[14] Kumar, N., Jain, P. K., Tandon, P., & Pandey, P. M. (2018). Extrusion-based additive manufacturing process for producing flexible parts. *Journal of the Brazilian Society of Mechanical Sciences and Engineering*, *40*(3), 143.

[15] Nieto, D. M., López, V. C., & Molina, S. I. (2018). Large-format polymeric pellet-based additive manufacturing for the naval industry. *Additive Manufacturing*, *23*, 79-85.

[16] Wang, X., Jiang, M., Zhou, Z., Gou, J., & Hui, D. (2017). 3D printing of polymer matrix composites: A review and prospective. *Composites Part B: Engineering*, *110*, 442-458.

[17] Alexandre, A., Cruz Sanchez, F. A., Boudaoud, H., Camargo, M., & Pearce, J. M. (2020). Mechanical Properties of Direct Waste Printing of Polylactic Acid with Universal Pellets Extruder: Comparison to Fused Filament Fabrication on Open-Source Desktop Three-Dimensional Printers. *3D Printing and Additive Manufacturing*.

[18] Khondoker, M. A. H., & Sameoto, D. (2020). *U.S. Patent Application No. 16/178,281*.

[19] Khondoker, M. A. H., & Sameoto, D. (2019). Direct coupling of fixed screw extruders using flexible heated hoses for FDM printing of extremely soft thermoplastic elastomers. *Progress in Additive Manufacturing*, *4*(3), 197-209.

[20] Khondoker, M. A. H., & Sameoto, D. (2016, November). Design and characterization of a bi-material co-extruder for Fused Deposition Modeling. In *ASME International*

Mechanical Engineering Congress and Exposition (Vol. 50527, p. V002T02A060). American Society of Mechanical Engineers.

[21] Singamneni, S., Smith, D., LeGuen, M. J., & Truong, D. (2018). Extrusion 3D printing of polybutyrate-adipate-terephthalate-polymer composites in the pellet form. *Polymers*, *10*(8), 922.

[22] Arunachalam, S., Gunasekaran, A., Ngum, S. M., Gill, K. F., & O'Sullivan, J. M. (1999). Taguchi-controlled knowledge-based assistant for improving quality of hollow cylindrical sections. *The International Journal of Advanced Manufacturing Technology*, *15*(7), 503-508.

[23] Ahn, S. H., Montero, M., Odell, D., Roundy, S., & Wright, P. K. (2002). Anisotropic material properties of fused deposition modeling ABS. *Rapid prototyping journal*, *8(4)*, 248-257.

[24] Halidi, S. N. A. M., & Abdullah, J. (2012, June). Moisture effects on the ABS used for Fused Deposition Modeling rapid prototyping machine. In *2012 IEEE Symposium on Humanities, Science and Engineering Research* (pp. 839-843). IEEE.

[25] O'Connor, A. E., & Willenbacher, N. (2004). The effect of molecular weight and temperature on tack properties of model polyisobutylenes. *International journal of adhesion and adhesives*, 24(4), 335-346.

[26] Barnes, H. A. (1997). Thixotropy - a review. *Journal of Non-Newtonian fluid mechanics*, *70(1-2)*, 1-33.

[27] Ya, F. R. E. N. K. E. L. (1980). Viscous flow of crystalline bodies under the action of surface tension. *SCI. SINTERING Sci. Sintering*, *12(1)*, 7.

[28] Bellehumeur, C., Li, L., Sun, Q., & Gu, P. (2004). Modeling of bond formation between polymer filaments in the fused deposition modeling process. *Journal of Manufacturing Processes*, *6(2)*, 170-178.

[29] Alaimo, G., Marconi, S., Costato, L., & Auricchio, F. (2017). Influence of meso-structure and chemical composition on FDM 3D-printed parts. *Composites Part B: Engineering*, *113*, 371-380.

Figures

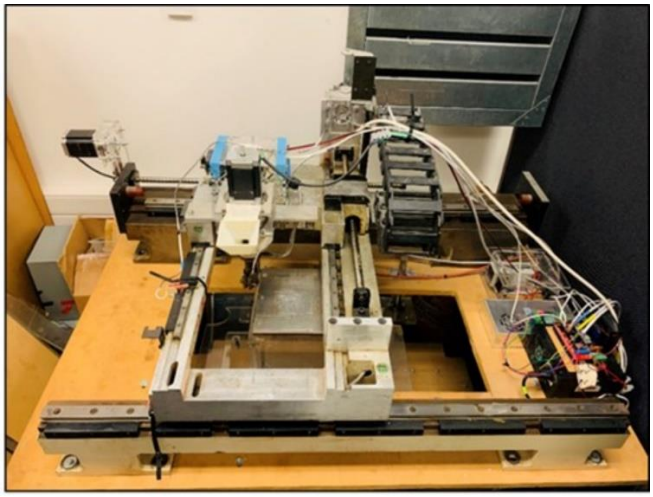

(a) Extrusion 3D printing set-up developed at AUT

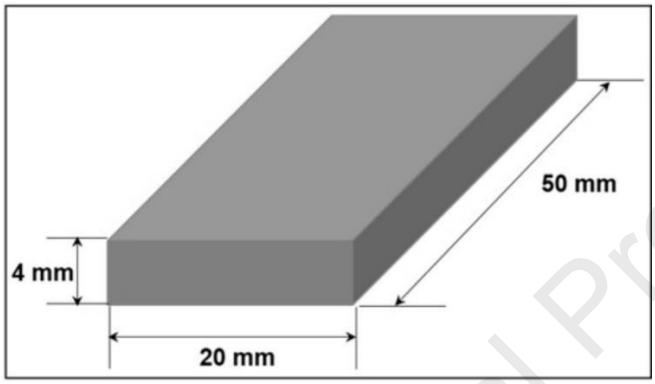

(b) CAD model of the samples to be printed

Figure 1. (a) Extrusion 3D printing set-up developed at AUT; New Zealand (b) CAD model of the samples produced

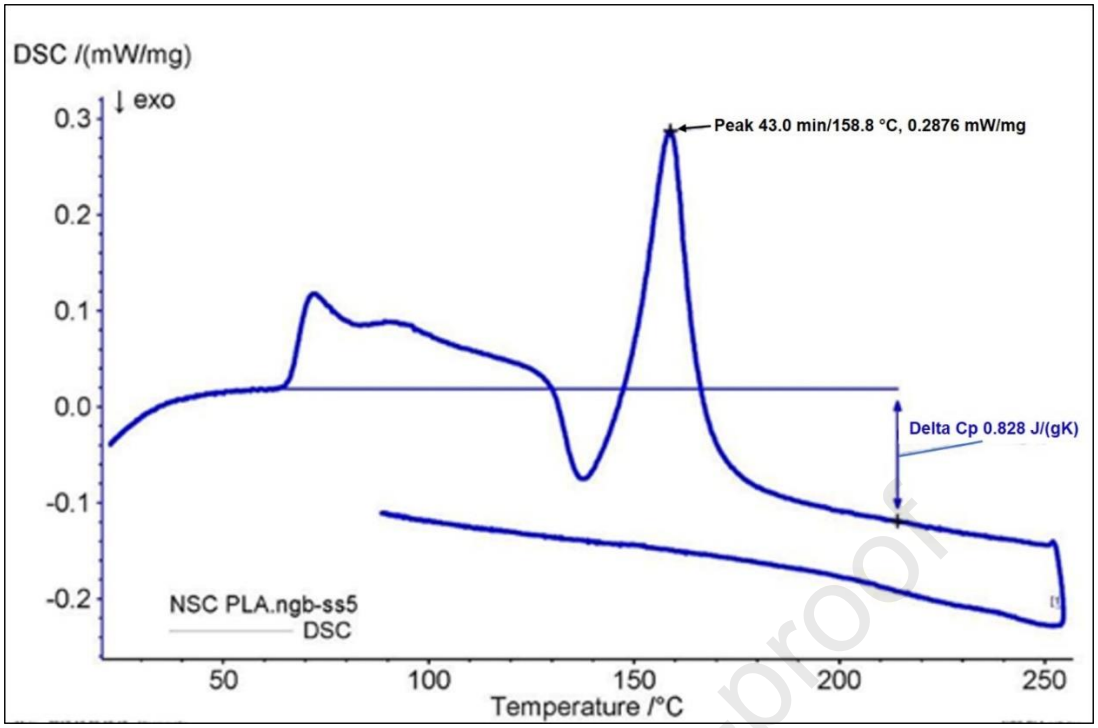

Figure 2. Differential scanning calorimetry (DSC) results

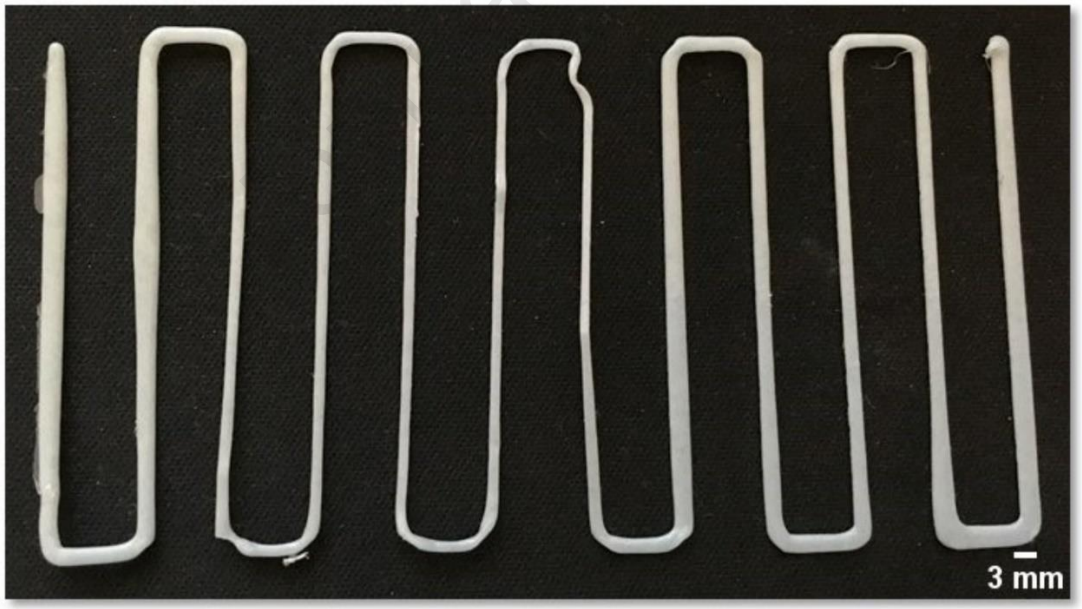

Figure 3. Single printed strands and continuity

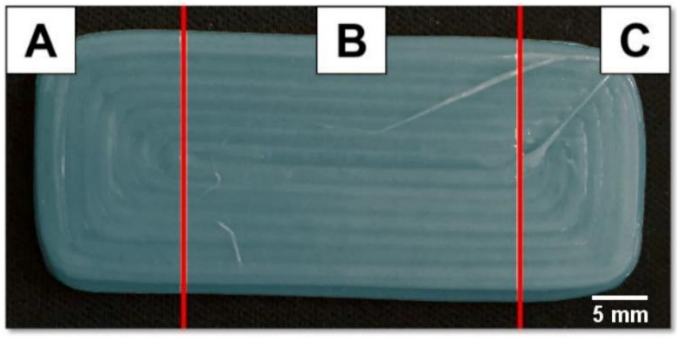

Figure 4. Raster path patterns and a single layer printed sample

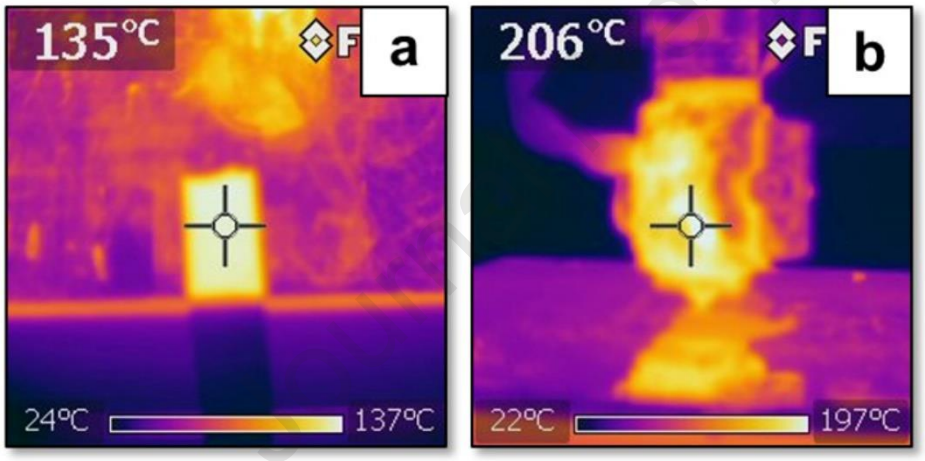

Figure 5. Infrared images(a) base plate, and (b) nozzle head.

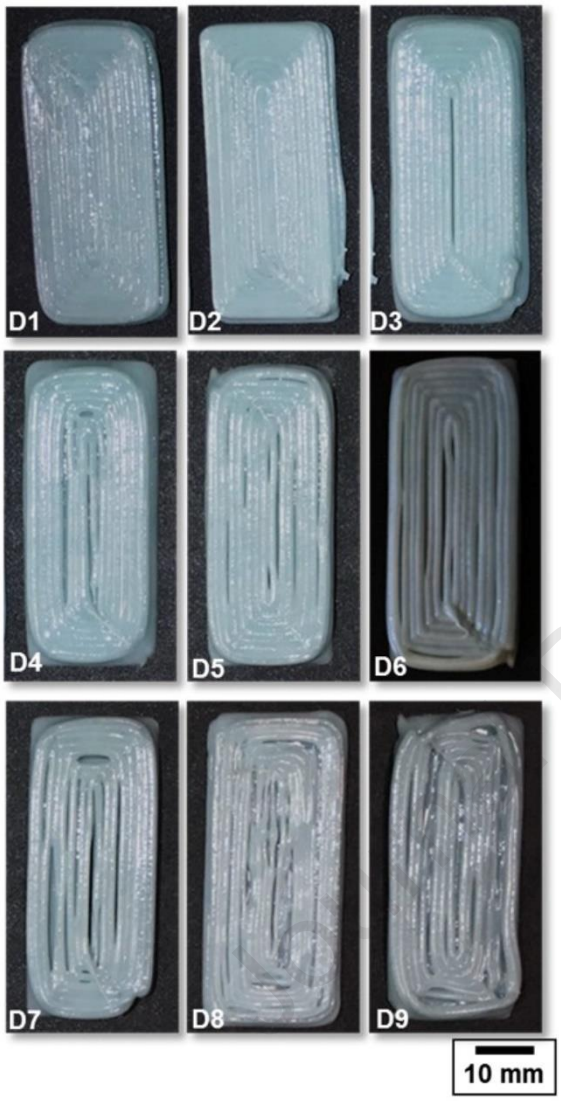

Figure 6. Multi-layer samples printed as per the design table.

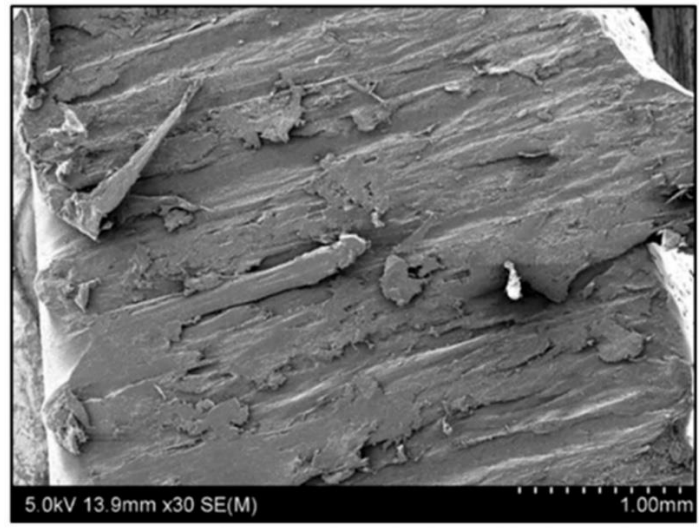

(a) Sectioned surface indicating resistance to splitting and strong polymerisation

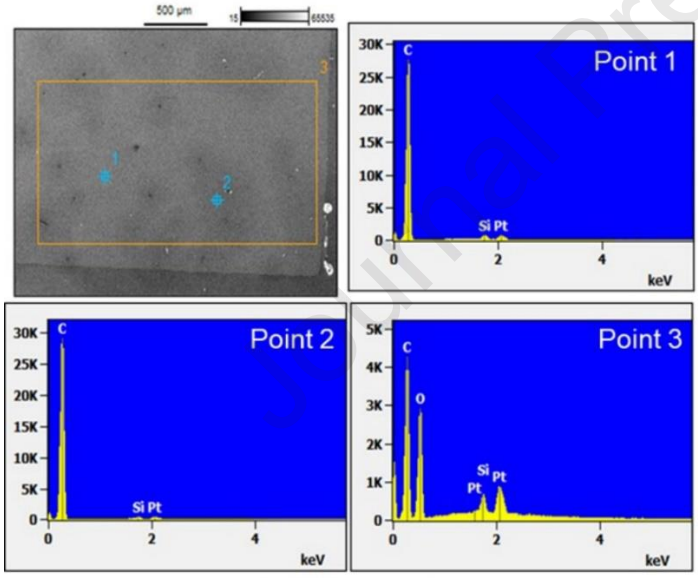

(b) EDS analysis

Figure 7. SEM analysis of the cross section of a representative printed specimen

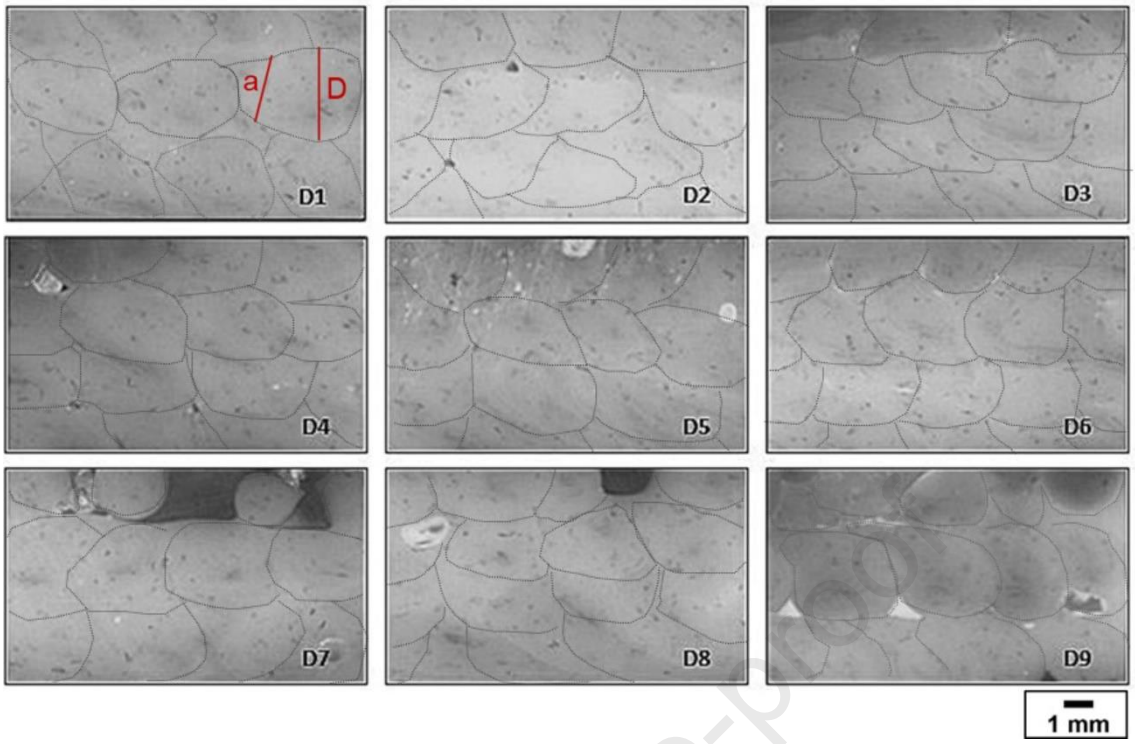

Figure 8. Meso structures of the cross sections of samples printed as per the experimental design

Figure 9. Samples after the three-point-bend test

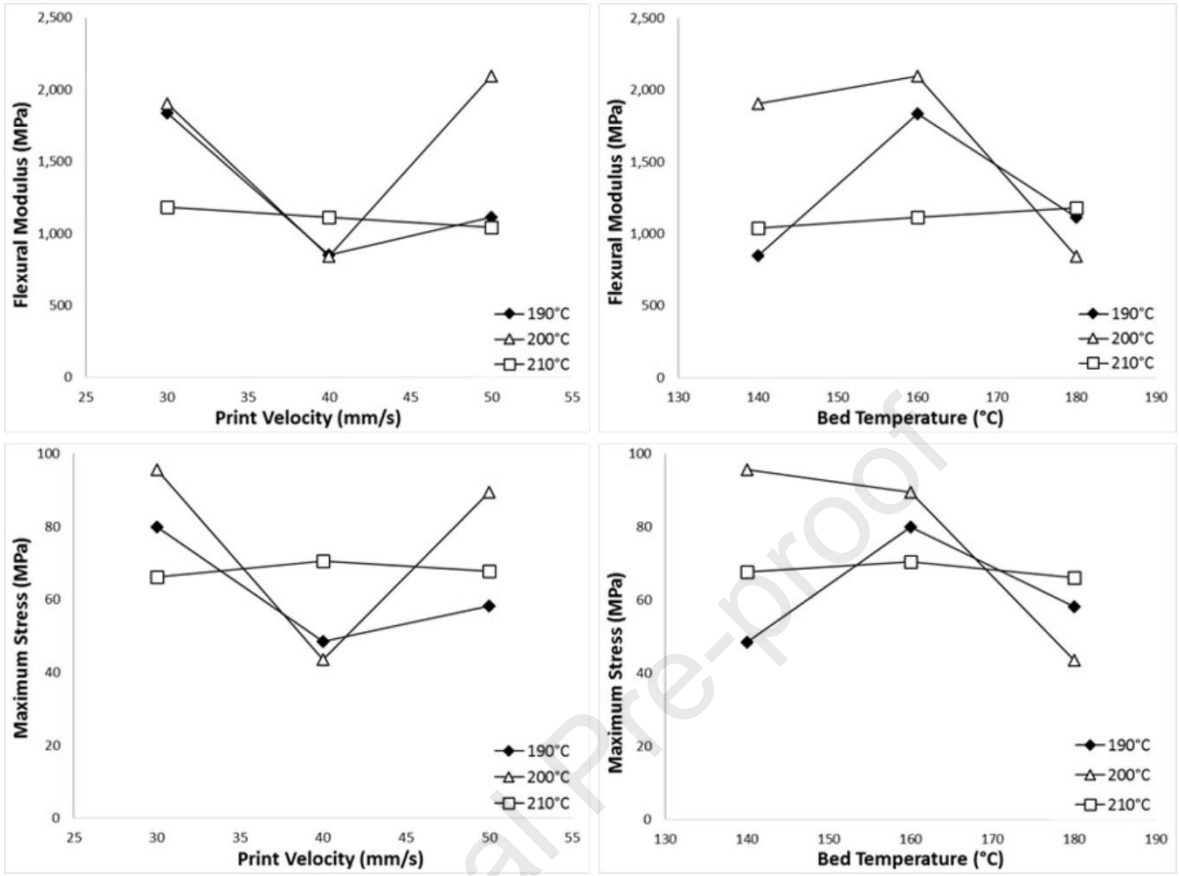

Figure 10. Flexural modulus and maximum stress responses against print velocity and bed temperature

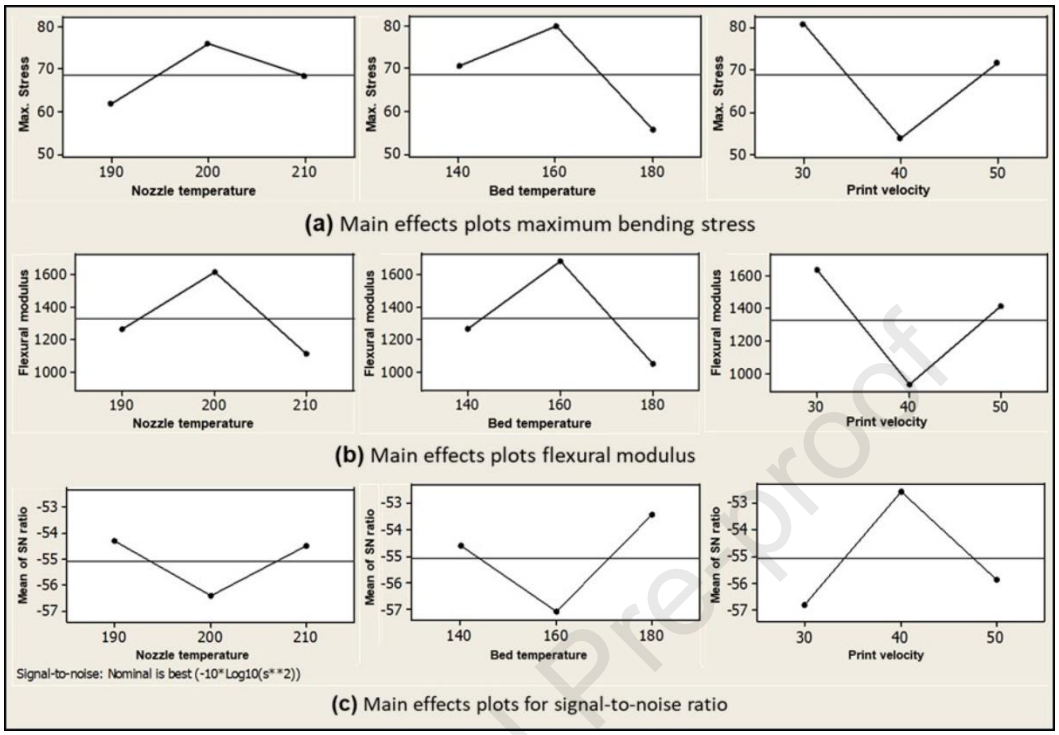

Figure 11. Main effects plots for mean (a) maximum bending stress and (b) flexural modulus (c) signal-to-noise ratio

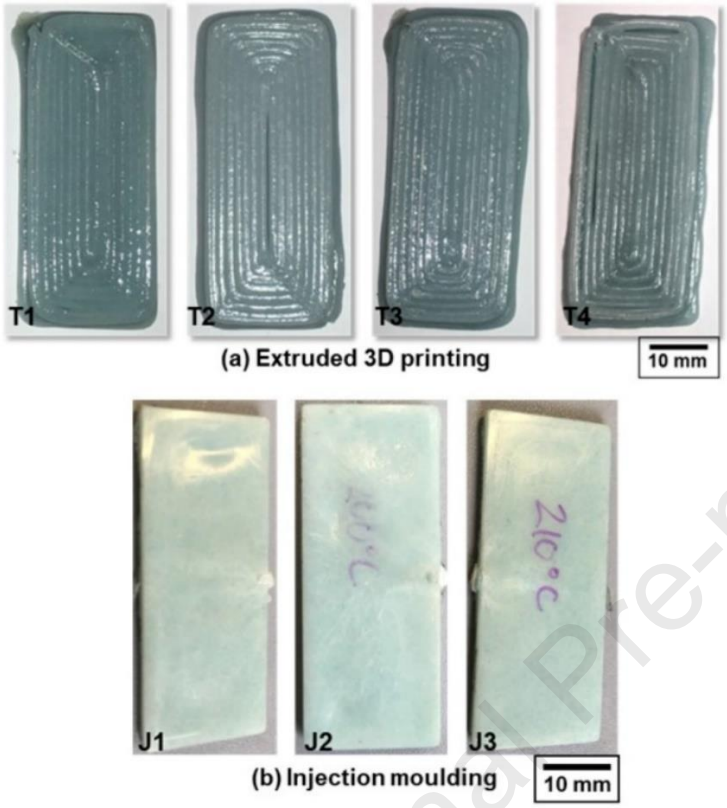

Figure 12. Three-point bending specimens produced by (a) extrusion 3D printing with nozzle temperature 200 °C, bed temperature 160 °C and print speed 30 mm/s (b) injection moulding with Nozzle temperatures 190 °C, 200 °C, and 210 °C.

Tables

Table 1. Taguchi L9 experimental design

No.	Nozzle Temp. (°C)	Bed Temp. (°C)	Print Velocity (mm/s)
D1	210	180	30
D2	210	160	40
D3	210	140	50
D4	200	180	40
D5	200	160	50
D6	200	140	30
D7	190	180	50
D8	190	160	30
D9	190	140	40

Table 2. Dimensional variations of samples printed as per the experimental design

No.	Thickness (%)	Width (%)	Length (%)	Coalescence (%)
D1	9.91	17.93	2.89	100
D2	9.71	11.23	4.80	88.71
D3	11.89	12.43	1.85	95.32
D4	13.79	13.76	0.10	86.72
D5	-10.80	8.21	-0.36	80.54
D6	-4.44	8.80	-1.46	98.43
D7	-13.64	10.91	-3.05	71.67
D8	-14.94	5.26	-1.69	79.23
D9	-0.25	5.26	-1.69	59.60

Table 3. Flexural test results and mechanical properties

No.	Force (N)	Maximum Deflection (mm)	Maximum Stress (MPa)	Maximum Strain	Flexural Modulus (MPa)
D1	848	1.8	66	0.0767	1,182
D2	831	2.0	71	0.0829	1,113
D3	851	1.9	68	0.0828	1,040
D4	579	1.5	43	0.0668	843
D5	677	1.7	89	0.0589	2,096
D6	820	1.7	96	0.0625	1,902
D7	432	2.1	58	0.0710	1,114
D8	545	1.7	80	0.0568	1,836
D9	434	2.0	48	0.0766	850

Table 4. Comparative responses of extrusion 3D printed and injection moulded samples

	Extrusion 3D printed					***Injection moulded***			
Sample no.	T1	T2	T3	T4	Avg.	J1	J2	J3	Avg.
Percent error in thickness	2.75	-3.50	1.75	-1.50	-0.125	0	0	0	0
Force (N)	577	822	680	598	669	581	621	451	551
Max. Deflection (mm)	1.5	1.8	1.3	1.4	1.5	1.6	1.55	1.25	1.47
Max. Stress (MPa)	63	69	67	65	66	68	73	53	65
Max. Strain	0.0215	0.0327	0.0245	0.2189	0.074	0.0614	0.0595	0.0480	0.056
Flexural Modulus (MPa)	1,516	1,447	1495	1410	1467	1,373	1,628	1,322	1441

Declaration of interests

☒ The authors declare that they have no known competing financial interests or personal relationships that could have appeared to influence the work reported in this paper.

☐The authors declare the following financial interests/personal relationships which may be considered as potential competing interests: